ACS APPLIED MATERIALS & INTERFACES

www.acsami.org

Research Article

Engineering of Biocompatible Coacervate-Based Synthetic Cells

Marleen H. M. E. van Stevendaal, Laurynas Vasiukas, N. Amy Yewdall, Alexander F. Mason,* and Jan C. M. van Hest*

Cite This: *ACS Appl. Mater. Interfaces* 2021, 13, 7879–7889

Read Online

ACCESS | Metrics & More | Article Recommendations | Supporting Information

ABSTRACT: Polymer-stabilized complex coacervate microdroplets have emerged as a robust platform for synthetic cell research. Their unique core–shell properties enable the sequestration of high concentrations of biologically relevant macromolecules and their subsequent release through the semipermeable membrane. These unique properties render the synthetic cell platform highly suitable for a range of biomedical applications, as long as its biocompatibility upon interaction with biological cells is ensured. The purpose of this study is to investigate how the structure and formulation of these coacervate-based synthetic cells impact the viability of several different cell lines. Through careful examination of the individual synthetic cell components, it became evident that the presence of free polycation and membrane-forming polymer had to be prevented to ensure cell viability. After closely examining the structure–toxicity relationship, a set of conditions could be found whereby no detrimental effects were observed, when the artificial cells were cocultured with RAW264.7 cells. This opens up a range of possibilities to use this modular system for biomedical applications and creates design rules for the next generation of coacervate-based, biomedically relevant particles.

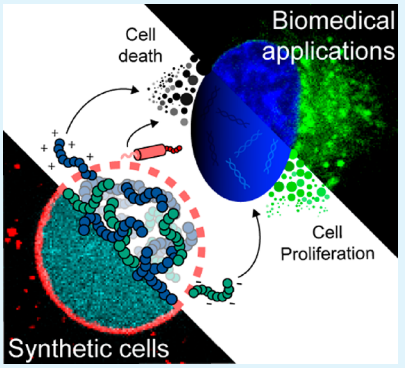

KEYWORDS: *complex coacervates, synthetic cells, polycations, biocompatibility, protocells, block copolymers, self-assembly*

INTRODUCTION

Complex coacervates have recently gained significant interest in the fields of cell biology,[1−3] synthetic cell engineering,[4−7] and biomedical applications.[8,9] They are liquid–liquid phase-separated compartments formed by synthetic or biological polyelectrolytes (e.g., polyacrylamides, polypeptides, and DNA). Their formation is driven by both an increase in entropy as a result of the release of counterions in solution and a decrease in enthalpy as a result of electrostatic interactions.[10,11] Complex coacervates are believed to have played an important role in the origin of life.[12] This has inspired scientists to utilize the self-assembling and crowded nature of coacervates to engineer synthetic cells[4] and artificial organelles,[13−15] which are capable of mimicking specific biological features including compartmentalization and communication.[5,16] A highly interesting characteristic of complex coacervates is their ability to host a great variety of so-called client molecules.[17] This characteristic has been exploited to encapsulate proteins and small molecules inside the coacervate phase to study biological processes in a simple and highly controlled environment.[17−21]

The ability to sequester high amounts of biologically relevant macromolecules is also important for the application of coacervate-based synthetic cells in the biomedical field. In fact, encapsulation of cargo in complex coacervates has already been demonstrated across a range of biomedical disciplines, including the development of sensors, biomimetic adhesives, and delivery platforms.[9] Encapsulation can be achieved by using the cargo as part of the coacervate matrix,[22] as a result of specific interactions,[18] or by preferential partitioning.[23−27] These methods result in the significant enrichment and protection of cargo inside the aqueous environment but also allow for their controlled release upon dissociation of the coacervate phase or as a reaction to external triggers. Overall, the development of programmable complex coacervate–synthetic cells shows great potential for creating novel delivery strategies, provided they are compatible with living cells.

Biocompatibility is thus a crucial design feature for coacervate formulations for in vitro and in vivo use and is closely linked to the choice of polymer that makes up the complex coacervate core. The relatively straightforward process of mixing oppositely charged polyelectrolytes has given rise to a broad range of materials that are being utilized for complex coacervation. These materials include polyanions (e.g., RNA,[28] ATP,[13] hyaluronic acid,[29] and heparin[26]) and polycations (e.g., diethylaminoethyl (DEAE) dextran,[30] poly(ethylene argininy-laspartate diglyceride) (PEAD),[26] and poly-L-lysine (PLL)[13,31]). However, not all of these materials are

Received: October 23, 2020
Accepted: February 5, 2021
Published: February 15, 2021

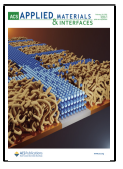

https://dx.doi.org/10.1021/acsami.0c19052
ACS Appl. Mater. Interfaces 2021, 13, 7879–7889

appropriate for cocultivation with biological cells, mostly due to their high charge.[32] Previous studies have reported the preparation of biocompatible coacervates through the use of natural polymers[27,33,34] or via careful design of synthetic polymers.[26,35,36] A disadvantage of most complex coacervates, however, is their inherent lack of long-term (>24 h) stability. In other words, there is little control over the coalescence of these droplets or their deposition on surfaces, which limits their use for long-term interactions with living cells.

In previous work, we reported on coacervate-based synthetic cells with a stabilizing block copolymer, which circumvents these processes.[37] More specifically, 12−16 kDa amylose chains were modified with a quaternary amine (Q) or a carboxymethyl (CM) group, introducing either a positive or negative charge on the amylose, respectively. Upon mixing, these charged polymers phase-separated into liquid coacervate droplets (Figure 1A). To terminate the growth of the droplets, a stabilizing synthetic block terpolymer was added that self-assembles around the droplet periphery. This biodegradable terpolymer, PEG−PCL-*g*-TMC−PGlu, comprises a poly(ethylene glycol) (PEG) chain that prevents internalization in the coacervate phase, a hydrophobic poly((ε-caprolactone)-*gradient*-trimethylene carbonate) (PCL-*g*-TMC) block that arranges the terpolymer around the droplet, and a negatively charged poly(glutamic acid) (pGlu) domain that interacts with the droplet periphery via electrostatic interactions.

The hierachical assembly of these synthetic cells allows for tuning of the properties of all of the different components, which enables control over the molecular interactions that dictate cargo sequstration and release.[18,23] However, the multicomponent assembly process induces a level of complexity that makes it more difficult to pinpoint biocompatibility issues. Progression of these coacervate-based synthetic cells in the field of biomedical applications can only be achieved when there is a clear understanding of their toxicity when in contact with living cells. The purpose of this study is to investigate how the structure and formulation of these coacervate-based synthetic cells impacts cell viability. Examination of the individual synthetic cell components revealed that the origin of initial synthetic cell toxicity could be attributed to the toxic character of free polycation and terpolymer. Careful examination of the structure−toxicity relationship disclosed a set of conditions whereby no detrimental effects were observed when cocultured with RAW264.7 cells. This study advances the development of synthetic cells for applications in a range of biomedical disciplines and outlines the criteria for the next generation of coacervate-based, biomedically relevant particle designs.

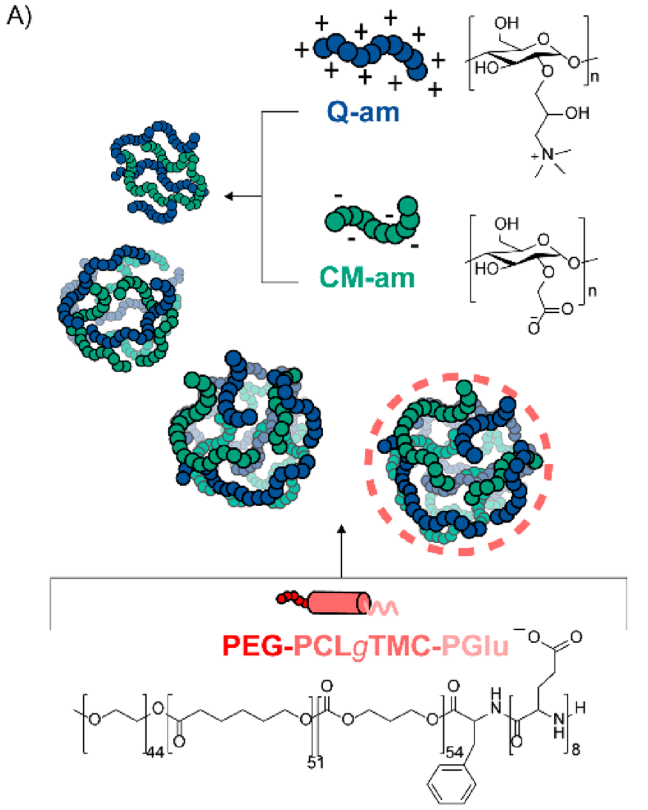

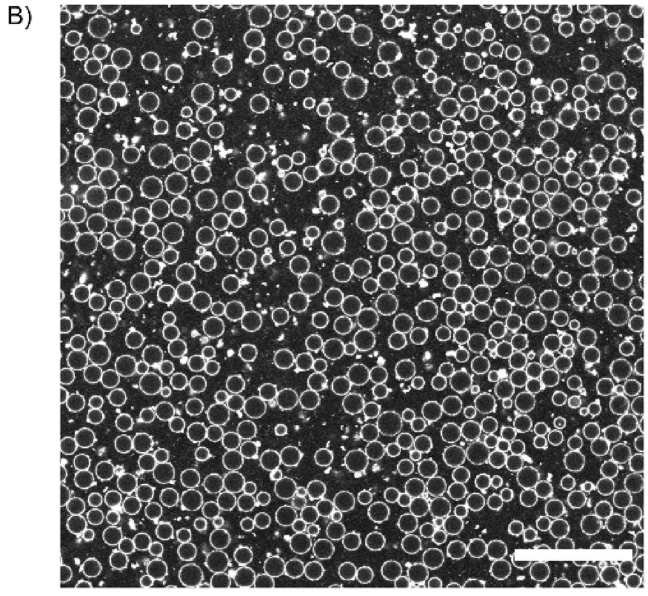

Figure 1. Self-assembly of stabilized coacervate-based synthetic cells. (A) Schematic illustrating the coacervation of the oppositely charged polycation (12−16 kDa) quaternary amylose (Q-am) and polyanion (12−16 kDa) carboxymethyl amylose (CM-am) followed by self-assembly of terpolymer poly(ethylene glycol)−poly(caprolactone-*gradient*-trimethylene carbonate)−poly(glutamic acid) (PEG−PCL-*g*-TMC−PGlu) on the droplet interface. (B) Confocal microscopy image of synthetic cells formed in cell culture medium. The terpolymer is visualized with Nile Red. Scale bar represents 50 μm.

MATERIALS AND METHODS

Materials. All chemicals were used as received unless otherwise stated. For the synthesis of the terpolymer, monomethoxy poly(ethylene glycol) 2 kDa was purchased from Rapp Polymere, trimethylene carbonate was purchased from TCI Europe, and dry methanesulfonic acid was kindly supplied by Arkema. For the preparation of modified amylose derivatives, amylose (12−16 kDa) was supplied by Carbosynth and 3-chloro-2-hydroxypropyltrimethylammonium chloride (65 wt % in water) was supplied by TCI Europe. For cell culture, Dulbecco's modified Eagle's medium (DMEM) (no. 41965062), fetal bovine serum (FBS) (no. 26140079), penicillin/streptomycin (no. 15140122), and trypsin-EDTA (0.05%) (no. 25300054) were purchased from Fisher Scientific. Vascular cell basal medium (VCBM) (no. 100-030) and Endothelial Cell Growth Kit-VEGF (no. 100-041) were purchased from LGC standards. Pacific Blue Annexin V Apoptosis Detection Kit with 7-AAD (no. 640926) was purchased from BioLegend. LysoTracker Green DND-26 (no. H3570), Hoechst 33342 (no. H3570), and Live Cell Imaging Solution (no. A14291DJ) were purchased from ThermoFisher Scientific. (All other chemicals were supplied by Sigma-Aldrich.)

https://dx.doi.org/10.1021/acsami.0c19052
ACS Appl. Mater. Interfaces 2021, 13, 7879−7889

Synthesis of Modified Amyloses. Both quaternized (Q-amylose) and carboxymethylated (CM-amylose) amyloses were prepared in accordance with previously published procedures.[37] In short, amylose was dissolved in a solution of aqueous NaOH prior to addition of either 3-chloro-2-hydroxypropyltrimethylammonium chloride solution (for Q-amylose) or chloroacetic acid (for CM-amylose). After the reaction, the reaction mixture was neutralized with acetic acid, precipitated into cold ethanol, and dialyzed extensively against Milli-Q before being lyophilized to yield CM-amylose (90% yield) or Q-amylose (80% yield) as fluffy white solids. The degrees of substitution were determined by ^{1}H NMR spectroscopy (Figure S1).

Synthesis of Cy5-Labeled Q-Amylose. First, amylose was modified in accordance with a previously published procedure to introduce an azido functional group at the reducing end.[38] Amylose (100 mg, 7.14 μmol, 1 equiv) was dissolved in 2.1 mL of deionized water containing *N*,*N*-diisopropylethylamine (93.3 μL, 536 μmol, 75 equiv) by heating to 95 °C in an oil bath. Once dissolved, the solution was cooled to room temperature and sodium azide (116 mg, 1.79 mmol, 250 equiv) was added, followed by 2-chloro-1,3-dimethylimidazolinium chloride (30.2 mg, 179 μmol, 25 equiv). The reaction mixture was left to stir at room temperature overnight. The product was purified via precipitation into cold ethanol, followed by extensive dialysis against Milli-Q before being lyophilized to yield azido amylose (91 mg, 91% yield) as a fluffy white solid. The introduction of the azide functionality at the reducing end was confirmed by the appearance of a new peak at 4.8 ppm by ^{1}H NMR spectroscopy. Prior to the conjugation of DBCO-Cy5, azido amylose was subjected to the same cationization protocol (described earlier) to yield azido-Q-amylose. For the labeling reaction, azido-Q-amylose (12 mg, 0.86 μmol, 10 equiv) was dissolved in 40 μL of Milli-Q, to which was added 10.3 μL of a dimethylformamide (DMF) solution of DBCO-Cy5 (10 mg/mL, 0.086 μmol, 1 equiv). The reaction was left to react overnight at room temperature, prior to precipitation in cold ethanol and lyophilization to yield a fluffy blue solid (25% yield, as determined by UV−vis spectroscopy).

Synthesis of Terpolymer. PEG−PCL-*g*-TMC−PGlu was prepared in accordance with previously published procedures.[37] In short, poly(ethylene glycol) monomethyl ether was used to initiate the ring-opening polymerization of ε-caprolactone and trimethylene carbonate. The terminal alcohol of this polymer was subsequently modified via a Steglich esterification with Boc-L-Phe-OH to yield a primary amine after trifluoroacetic acid (TFA) deprotection. The final poly(L-glutamic acid) block was introduced by the ring-opening polymerization of *N*-carboxyanhydride γ-benzyl L-glutamate, followed by hydrogenation. At each step, the polymer modifications were confirmed by both GPC and ^{1}H NMR (Figures S11 and S12).

Synthesis of Dy650-Labeled Terpolymer. PEG−PCL-*g*-TMC−PGlu−NH_2 (10 mg, 0.77 μmol, 10 equiv) was dissolved in 10 μL of DMF, to which was added 8.2 μL of a DMF solution of DyLight650-NHS ester (10 mg/mL, 0.08 μmol, 1 equiv). The reaction was left to react overnight at room temperature prior to precipitation in cold methanol (twice) and lyophilization from dioxane to yield a gummy blue solid (54% yield, as determined by UV−vis spectroscopy). The unlabeled terpolymer was not separated from the Dy650 terpolymer, as it was diluted further with terpolymer for the cell experiments anyway.

Preparation of Coacervates. Q-amylose with degrees of substitution (DS) of 1 and 0.5 and CM-amylose with a DS of 0.4 were dissolved separately in cell culture medium (DMEM, supplemented with 10% (v/v) FBS and 1% (v/v) penicillin/streptomycin or VCBM, supplemented with Endothelial Cell Growth Kit-VEGF) (Table 1). Coacervation was induced by the addition of Q-amylose (50 μL) to CM-amylose (50 μL) in molar charge ratios 1:1, 1:2, and 1:3 while shaking at 1400 rpm. After 7 min, terpolymer (5 or 2 μL, 25 mg mL^{-1} in PEG350) was added.

Purification of Coacervates. Coacervates were purified by centrifugation at 500*g* for 4 min, after which the supernatant was carefully removed and transferred to a new Eppendorf tube. The viscous pellet was redissolved in an equal volume of cell culture medium.

Table 1. Concentrations of Amyloses Dissolved in Cell Culture Medium for Different Molar Charge Stoichiometries

molar charge ratio ($[Q]^+/[CM]^-$)	[Q-amylose] (μg mL^{-1})	[CM-amylose] (μg mL^{-1})
	Q-amylose DS 1.0	
1:1	1000	1670
2:1	1000	830
3:1	1000	550
	Q-amylose DS 0.5	
1:1	1000	1050
2:1	1000	530
3:1	1000	350

Cell Culture. HeLa cells and RAW 264.7 macrophages were grown as a monolayer in DMEM and supplemented with 10% (v/v) FBS and 1% (v/v) penicillin/streptomycin in a humidified atmosphere of 5% CO_2 at 37 °C. Human umbilical vein cells (HUVECs) were grown as a monolayer in VCBM and supplemented with Endothelial Cell Growth Kit-VEGF in a humidified atmosphere of 5% CO_2 at 37 °C.

Cell Viability Assay. The toxicity of coacervates and its components was evaluated using an Annexin V/7AAD apoptosis assay. Two days prior to measuring cell viability, cells were seeded in 96-well plates and grown to 60−70% cell confluency overnight. The following day, cells were incubated with Q-amylose, CM-amylose, terpolymer, and coacervates. After 24 h of incubation, the cell medium was collected and the cells were washed three times with phosphate-buffered saline (PBS), which was also collected. Subsequently, the cells were harvested using trypsin and washed three times with PBS supplemented with EDTA (2 mM) and 2% v/v FBS, prior to the addition of annexin binding buffer and incubation with Annexin V and 7-AAD staining solution for 15 min in the dark at room temperature. Samples were analyzed by flow cytometry using a BD FACSAria III (Becton Dickinson) and FACSDiva Software (Becton Dickinson). 7-AAD was excited at 561 nm, and emission was recorded between 650 and 690 nm. Pacific Blue labeled Annexin V was excited at 405 nm, and emission was recorded between 418 and 482 nm. Single cells were gated based on their forward and sideward scatter. The percentage of viable cells was normalized to the positive control, which was ≥75% for all samples. For each sample, >1000 cells were recorded.

Confocal Microscopy for Visualizing Cellular Uptake. One day prior to the addition of DyLight650-labeled terpolymer or Cy5-labeled Q-amylose, 40.000 HeLa cells or 120.000 RAW264 cells were seeded in an 8-well μ-ibiTreat slide (Ibidi). The next day, the medium was replaced with fresh medium containing 1250 μg/mL terpolymer or 250 μg/mL Q-amylose. After 4 h of incubation in a humidified atmosphere of 5% CO_2 at 37 °C, the medium was aspirated, and the cells incubated with terpolymer were washed two times with PBS. Cells were stained with a colocalization marker for lysosomes, LysoTracker Green, and nuclear marker Hoechst 33342 for 20 min. Cells were imaged in Life Cell Imaging Solution using a Leica TCS SP5 confocal microscope equipped with an HCX PL Apo CS 63×/1.20 UV−vis−IR water-immersion objective and PMT detector. The pinhole was set to 1 Airy Unit. Images (1024 × 1024 pixels) were acquired with a scan rate of 200 Hz and line-averaged three times. DyLight650 and Cy5 were excited at 650 nm, and emission was recorded between 670 and 780 nm. Hoechst 33342 was excited at 405 nm, and emission was recorded between 415 and 450 nm. LysoTracker Green was excited at 500 nm, and emission was recorded between 525 and 600 nm. Images of two independent experiments (N = 2) were analyzed using Fiji (ImageJ).

Confocal Microscopy of Coacervates. Coacervates were prepared using Nile Red to stain the terpolymer membrane (1% v/v) or loaded with Cy5-labeled succinylated bovine serum albumin (BSA) and subsequently transferred to an 18-well μ-slide (Ibidi). Imaging of coacervates was performed using a Leica TCS SP5

https://dx.doi.org/10.1021/acsami.0c19052
ACS Appl. Mater. Interfaces 2021, 13, 7879−7889

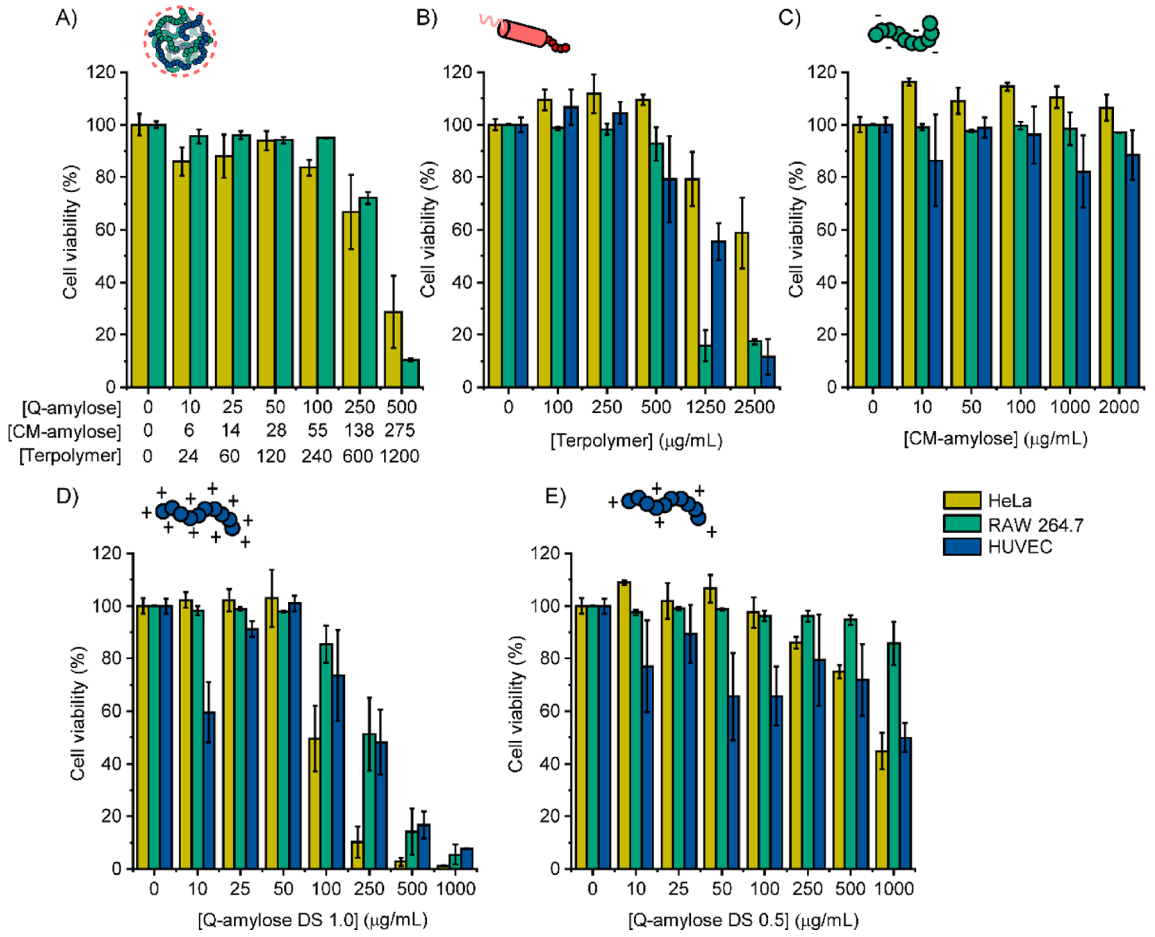

Figure 2. Toxicity of coacervates and their components. Cell viability of HeLa cells, RAW264.7 macrophages, and human umbilical vein endothelial cells (HUVECs) after 24 h of incubation with (A) coacervates, (B) terpolymer, (C) CM-amylose with a degree of substitution (DS) of 0.4, (D) Q-amylose$_{DS=1.0}$, and (E) Q-amylose$_{DS=0.5}$. Error bars represent the standard deviation of 2 independent experiments.

confocal microscope equipped with an HCX PL Apo CS 63×/1.20 UV−vis−IR water-immersion objective and PMT detector. The pinhole was set to 1 Airy Unit. Images (1024 × 1024 pixels) were acquired with a scan rate of 200 Hz and line-averaged six times. Nile Red was excited at 550 nm (75% laser power), and emission was recorded between 570 and 620 nm. Cy5 was excited at 649 nm, and emission was recorded above 670 nm. Images were analyzed using Fiji (ImageJ). The size and fluorescence distribution were determined using standard ImageJ functions. The particles were selected by thresholding the image and converting it into a binary image, using "manual thresholding". Overlapping images in the binary image were separated using the "watershed" function. Subsequently, the particles were analyzed using "particle analysis". Particles on the edge of the image were excluded from the analysis. A minimum of 200 particles were analyzed per image.

Turbidity Measurements. Coacervates were prepared as previously described with different molar charge stoichiometries. For turbidity measurements the terpolymer was omitted. Absorption measurements were performed on a Tecan Spark 10 M plate reader. The turbidity of the coacervate solutions was subsequently calculated as $100 - \%T = 100 - (100 \times 10^{-\mathrm{Abs500}})$.

^{1}H NMR Analysis. Q-amylose with degrees of substitution (DS) of 0.5 or 1 and CM-amylose with a DS of 0.4 were dissolved separately in PBS. Coacervates were prepared as previously described with different molar charge ratios. Coacervates were then centrifuged at 500*g* for 4 min, after which the supernatant was transferred to a new Eppendorf tube and the pellet was redissolved in PBS. The samples were subsequently freeze-dried overnight and redissolved in D_2O (to measure Q- and CM-amylose) or dimethyl sulfoxide (DMSO-d_6) (to measure terpolymer). Samples were centrifuged at 17 000*g* for 10 min, and the supernatant was characterized with ^{1}H NMR spectroscopy (400 MHz). As a control, the same amount of polymer was dissolved in D_2O or deuterated DMSO and characterized with ^{1}H NMR spectroscopy. Unique compound peaks were integrated using MestreNova and were used to calculate the ratio and concentration of polymer in the pellet and supernatant.

RESULTS AND DISCUSSION

Preparation of Terpolymer-Stabilized, Coacervate-Based Synthetic Cells in a Biologically Relevant Medium. The first challenge in applying this synthetic cell system in biomedical applications is their stability in a biological environment because the phase separation of polymers is dictated by buffer parameters, such as pH and ionic strength.[10] Coacervate microdroplets comprising Q-amylose and CM-amylose have been reported to form at physiological pH (7.4), with a critical salt concentration (NaCl) of 440 mM.[37] However, it is unknown whether these particles also form in a complex and biologically relevant environment like cell culture medium (e.g., DMEM supplemented with serum), which is characterized by the presence of many divalent salts (e.g., $CaCl_2$ and $MgSO_4$), vitamins, polysaccharides, amino acids, and proteins (e.g., growth factors). To this end, Q-amylose and CM-amylose were dissolved separately in cell culture medium and mixed for several minutes, upon which these charged polymers phase-separated from the original dispersion into liquid coacervate

https://dx.doi.org/10.1021/acsami.0c19052
ACS Appl. Mater. Interfaces 2021, 13, 7879−7889

droplets. After addition of the terpolymer PEG−PCL-*g*-TMC−PGlu, discrete polydisperse particles were formed in cell culture medium, which could then be directly used for culturing experiments with cells (Figure 1B). Importantly, coacervate-based synthetic cells prepared in cell culture medium displayed stability for an extended time of at least 9 days in a humidified incubator at physiological conditions (5% CO_2 at 37 °C) while retaining their fluorescent cargo, size, and spherical morphology (Figure S2).[39] These results emphasize the robustness of this platform for applications in a range of biomedically relevant situations.

Toxicity Evaluation of Coacervates and Their Components, Terpolymer and Quaternary and Carboxymethyl Amyloses. Besides stability in a biologically relevant environment, biocompatibility of complex coacervates is crucial for establishing cellular interactions. To determine whether coacervates or their components induced any cytotoxicity, plasma membrane damage was assessed by determining Annexin-V and 7-AAD positive cells. Annexin V targets phosphatidyl serine, which is located on the intracellular leaflet of the plasma membrane in healthy cells. Because membrane asymmetry is lost during apoptosis, phosphatidyl serine is exposed on the membrane surface where fluorescently labeled Annexin V can bind. 7-AAD binds DNA but is excluded from healthy cells; when cells are late apoptotic or necrotic, 7-AAD can enter the nucleus.[40] Different cell types were included in this study: a human cancer cell line (HeLa), a murine macrophage line (RAW264.7), and a human umbilical vein endothelial cell line (HUVEC).

First, coacervate microdroplets were prepared in cell culture medium and cocultivated with cells to determine their biocompatibility. Initially, coacervates were prepared following a previously described formulation using Q-amylose with a degree of substitution (DS) of ≥0.8 (Q-amylose$_{DS\geq0.8}$), CM-amylose with a DS of 0.4 (CM-amylose$_{DS=0.4}$), and a charge stoichiometry ($[Q]^+/[CM]^-$) of 3 (Figure S1).[37] The DS of Q-amylose or CM-amylose represents the number of hydroxyl groups per amylose unit that are substituted for a quaternary amine or a carboxymethyl group, respectively. The charge stoichiometry represents the ratio between the number of positive and negative charges present in the formulation. The solvent in which the terpolymer PEG−PCL-*g*-TMC−PGlu was originally dissolved was changed from DMSO to the more biocompatible and biologically inert PEG350 to circumvent the toxic effects reported for DMSO.[41,42] For this purpose, freeze-dried solid terpolymer was dissolved in PEG350. Exposing cells to different concentrations of these coacervate-based synthetic cells decreased cell viability by 35% for HeLa cells and 30% for RAW264.7 macrophages when exceeding concentrations of 100 μg mL^{-1} Q-amylose$_{DS=1.0}$, 60 μg mL^{-1} CM-amylose$_{DS=0.4}$, and 240 μg mL^{-1} terpolymer (Figure 2A).

To determine the origin of the observed coacervate toxicity, the biocompatibilities of the separate coacervate components were evaluated. Cells were incubated with different concentrations of terpolymer PEG−PCL-*g*-TMC−PGlu, which led to plasma membrane damage when exceeding a concentration of 500 μg mL^{-1} (Figure 2B). More specifically, LC_{50} values revealed that the terpolymer was most toxic for RAW264.7 cells (LC_{50} < 1250 μg mL^{-1}), followed by HUVECs (LC_{50} < 2500 μg mL^{-1}) and HeLa cells (LC_{50} > 2500 μg mL^{-1}). RAW264.7 cells are known to phagocytose anionic particles and compounds, which might result in intracellular accumulation at a high concentration. The exact mechanism of toxicity of this group of polymers is still unknown; however, intracellular overloading of polymeric nanoparticles has been proposed to damage the lysosomal compartment, eventually resulting in cell death.[43] To investigate this possibility and thereby explain the difference in toxicity between RAW264.7 cells and HeLa cells, cellular uptake studies of terpolymer labeled with DyLight650 were performed. Indeed, RAW264.7 macrophages internalized more terpolymer inside the lysosomes than HeLa cells, thereby supporting this hypothesis (Figure S3).

Different terpolymer batches displayed higher toxicity for HeLa cells (LC_{50} < 2500 μg mL^{-1}) but similar toxicity for RAW264.7 cells (LC_{50} < 1250 μg mL^{-1}) (Figure S4). Studies using a similar polymer (PEG−PCL-*g*-TMC) in nanoparticle formulations reported comparable toxicities for different cell lines.[44,45] These data indicate that the reduced biocompatibility of the coacervate could be a direct consequence of terpolymer toxicity.

Next, the two polyelectrolytes, CM-amylose and Q-amylose, were dissolved in cell culture medium and incubated with cells. A typical concentration for CM-amylose and Q-amylose in a coacervate-based synthetic cell formulation is 250−500 μg mL^{-1}. Importantly, CM-amylose did not influence cell viability up to 2000 μg mL^{-1} (Figure 2C). Moreover, Q-amylose did not influence cell viability up to a concentration of 50 μg mL^{-1} (Figure 2D). However, upon increasing the concentration of Q-amylose, cell viability sharply decreased as demonstrated by LC_{50} values of Q-amylose <100 μg mL^{-1} for HeLa cells and LC_{50} < 250 μg mL^{-1} for RAW264.7 cells and HUVECs. HeLa cells appeared to be most prone to Q-amylose toxicity, whereas RAW264.7 cell viability was less affected. In contrast to the terpolymer, accumulation in the lysosomal compartments did not contribute to this difference, as similar uptake was observed inside RAW264.7 and HeLa cells (Figure S5). RAW264.7 cells are thus not inclined to take up these positively charged polymers. This is in line with observations that phagocytotic cells like RAW264.7 cells preferably interact with anionic particles, presumably due to their function as bacteria scavengers, which also display a net negative charge.[46] These data suggest that another mechanism is responsible for Q-amylose toxicity. In an attempt to better understand and overcome cytotoxicity induced by Q-amylose, the structure−toxicity relationship of polycations was more closely examined.

Many commercially available polycations (e.g., poly-L-lysine (PLL), poly(ethylene imine) (PEI), poly(allyl amine) (PAH), and poly(diallyl dimethylammonium) (PDDA)) display toxicity at comparable concentrations, limiting the scope of these polycations for biological applications of complex coacervates.[47,32] Fortunately, the synthesis of biocompatible polycations has also been reported.[35,36] When designing such a biocompatible polycation, understanding the mechanism of toxicity is important but difficult to elucidate. Previous studies describe pore formation in the phospholipid bilayers of the cell membrane and mitochondrial disfunction as possible mechanisms for cellular toxicity.[48,49] Moreover, toxicity is influenced by different properties of polycations including (i) molecular weight, (ii) charge density and type of cationic functionality, (iii) structure (linear vs branched), and (iv) conformational flexibility or rigidity. The former two define the reactivity of the polycation, whereas the latter two determine the accessibility of the charge to the cell membrane. The toxicity originating from Q-amylose could thus be ascribed to its

https://dx.doi.org/10.1021/acsami.0c19052
ACS Appl. Mater. Interfaces 2021, 13, 7879−7889

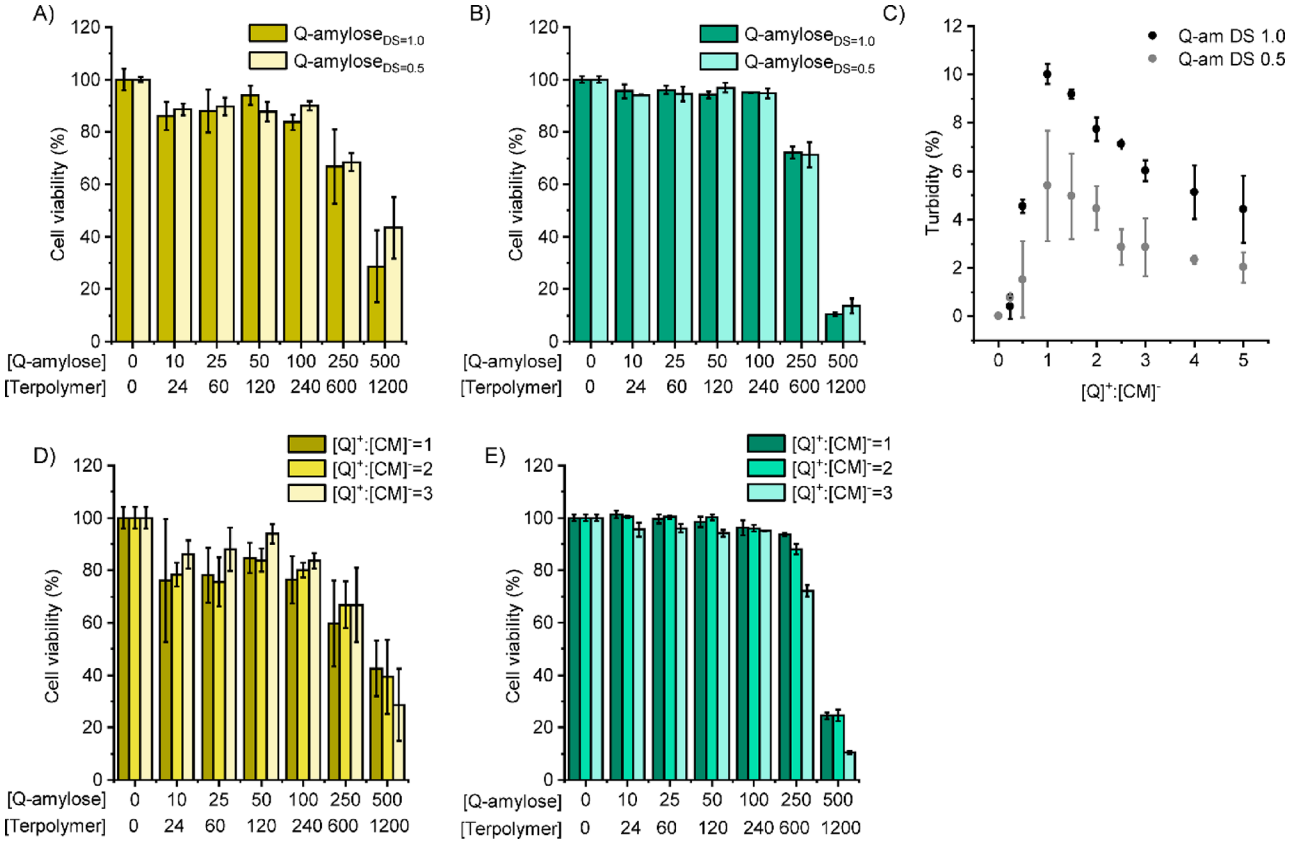

Figure 3. Toxicity of terpolymer-stabilized, coacervate-based synthetic cells. (A, B) Cell viability after 24 h of incubation with entire synthetic cell mixtures prepared with either Q-amylose$_{DS=1.0}$ or Q-amylose$_{DS=0.5}$ for (A) HeLa and (B) RAW264.7 cells. (C) Turbidity measurements of coacervates with different molar charge ratios prepared in cell culture medium. (D) Cell viability after 24 h of incubation with entire synthetic cell mixtures prepared with Q-amylose$_{DS=1.0}$ and molar charge ratios ([Q]$^+$/[CM]$^-$) of 1, 2, and 3 for (D) HeLa cells and (E) RAW264.7 cells. Concentrations on the *x*-axis are given in μg mL^{-1}. Error bars represent the standard deviation of 2 independent experiments.

flexible structure, high molecular weight, and high charge density. Charge density is dependent on the number of hydroxyl groups per amylose unit that are substituted for a quaternary amine (DS). Interaction of Q-amylose with the cell membrane might be key to explaining the difference between toxicity for HeLa and RAW264.7 cells. Cancer cells generally have increased glycolytic metabolism, resulting in a more negatively charged plasma membrane and thus stronger interaction with cationic compounds.[50] To further investigate this hypothesis, additional studies are required in the future.

To decrease Q-amylose toxicity, a new polymer was synthesized with a DS of 0.5 (Q-amylose$_{DS=0.5}$) that has a lower charge density (Figure S1B and C). After exposing cells to Q-amylose$_{DS=0.5}$, LC_{50} increased to >500 μg mL^{-1} for HeLa cells and HUVECs and to >1000 μg mL^{-1} for RAW264.7 cells (Figure 2E). These data imply that the dense positive charge of the original Q-amylose$_{DS=1.0}$ indeed influenced cell viability. Overall, lowering the DS of Q-amylose represents a good method to decrease polycation toxicity and points to Q-amylose$_{DS=0.5}$ as the better choice regarding future biomedical applications using coacervate-based synthetic cells.

Engineering of the Coacervate-Based Synthetic Cell Formulation. After establishing the role in cell toxicity of the individual components, the toxicity of the entire formulation was evaluated and regulated. In a first attempt to improve cell viability, the destructive interaction of positive charges with the plasma membrane was addressed. Indeed, Q-amylose free in solution is more toxic than Q-amylose phase-separated with CM-amylose, as the positive charge of Q-amylose is counterbalanced by the negatively charged CM-amylose.

However, it is possible that not all positive charge is compensated, resulting in cell membrane damage and eventual cell death induced by residual charge. To study this, coacervates were prepared with the less toxic Q-amylose$_{DS=0.5}$ (Figure S6B). Interestingly, the cell viability did not improve for both cell lines (Figure 3A and B). To address the possibility of free Q-amylose in the dilute phase affecting cell viability, due to excess Q-amylose in coacervate preparation, coacervates were prepared with different charge stoichiometries. The charge stoichiometry is one of the most significant parameters associated with complex coacervation. Previous studies have reported a maximum of coacervate formation for polymers of equal length and equal charge, when the number of charges from the polyanion is identical to the number of charges from the polycation.[10] This composition corresponds to a state of charge neutrality with the least free polymers in solution. In the original composition, an excess of positive charge (Q-amylose) was added to the synthetic cells, to ensure a net positive charge on the coacervates and consequent anchoring of the terpolymer on the particle surface. However, maximum coacervation, measured by the turbidity of the solution, was observed at [Q]$^+$/[CM]$^-$ = 1 (Figure 3C). Coacervate-based synthetic cells were prepared with different charge stoichiometries varying from 1 to 3 and added to HeLa and RAW264.7 cells. Importantly the coacervates were still stabilized by the terpolymer in these compositions (Figure S6A, C, and E).

https://dx.doi.org/10.1021/acsami.0c19052
ACS Appl. Mater. Interfaces 2021, 13, 7879−7889

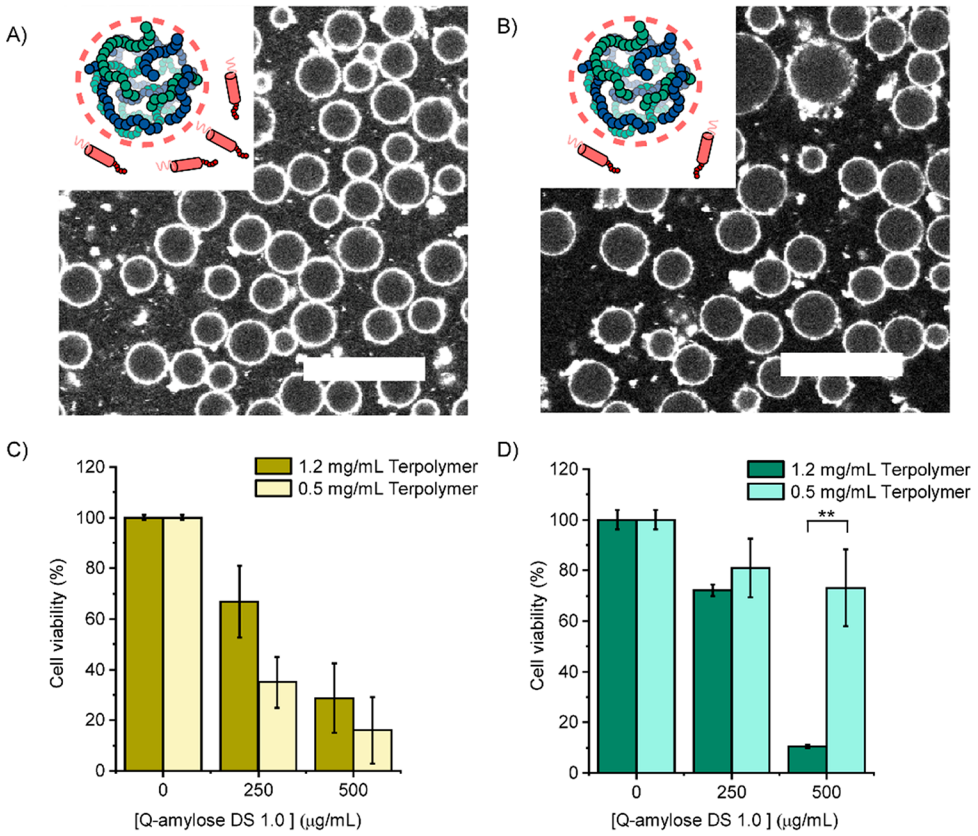

Figure 4. Terpolymer-dependent, coacervate-based synthetic cell toxicity. (A) Confocal microscopy image of coacervates prepared using 1.2 mg mL^{-1} terpolymer (final concentration) or (B) 0.5 mg mL^{-1} terpolymer (final concentration). The terpolymer is visualized with Nile Red. Scale bar represents 25 μm. (C, D) Cell viability after 24 h of incubation with synthetic cells for (C) HeLa cells or (D) RAW 264.7 cells. $[Q]^+/[CM]^- = 3$, $Q\text{-amylose}_{DS=1.0}$. The final terpolymer concentration is 1.2 or 0.5 mg mL^{-1}. Error bars represent the standard deviation of 2 independent experiments. Significance was assessed using the Student's t test. Significance level is indicated by $^{**}p < 0.05$.

Surprisingly, lowering the charge stoichiometry did not affect HeLa cell viability and improved the cell viability of RAW264.7 cells only by maximally 15% (Figure 3D and E). This trend was independent of the DS of Q-amylose (Figures S7 and S6B, D, and F). These data suggest a toxicity mechanism that is independent of the charge stoichiometry of the coacervate formulation, either because of an excess of positive charge in the dilute phase or by an excess of terpolymer.

In a second attempt to recover cell viability, the role of the terpolymer in the toxicity of coacervate-based synthetic cells was assessed. Arrangement of terpolymer PEG−PCL-*g*-TMC−PGlu on the synthetic cell surface was hypothesized to primarily expose cells to PEG_{44}, which has been reported to be nontoxic up to 20 mg mL^{-1}.[41] However, in previous reports, an excess of terpolymer was added to coacervates to ensure stabilization.[37] Indeed, reducing the final terpolymer concentration from 1200 to 500 μg mL^{-1} was revealed to be sufficient to stabilize coacervates without obvious coalescence or size increase (Figure 4A and B). However, decreasing the terpolymer concentration from 1.2 to 0.5 mg mL^{-1} unexpectedly increased HeLa cell toxicity (Figure 4C). A possible explanation is the diffusion of Q-amylose from the coacervate phase to the original dispersion, as a result of lower long-term stabilization by the terpolymer. Lowering the charge stoichiometry and DS decreased this difference in cytotoxicity, supporting this hypothesis (Figure S8A and C). In contrast, lowering the terpolymer concentration returned the cell viability of RAW264.7 macrophages to 75% (Figure 4D), suggesting a prominent role for the terpolymer in the toxicity of RAW264.7 cells. This was independent of the charge stoichiometry and DS (Figure S8B and D). HeLa cells internalize the terpolymer to a lesser extent than RAW264.7 macrophages (Figure S3), which explains why decreasing its concentration had no positive effect on HeLa cell viability.[51]

All together, these data imply a different toxicity mechanism for Hela cells and RAW 264.7 macrophages, as was also suggested by the toxicity evaluation of the separate compounds. A combination of free Q-amylose and terpolymer might play a prominent role in coacervate-based synthetic cell toxicity for HeLa cells, whereas an excess of terpolymer could play the most prominent role in RAW264.7 toxicity.

Removal of Free Polymers by Purification. Finally, we investigated whether the observed toxicity toward cells was an intrinsic feature of the coacervates or a result of residual polymer free in solution, which did not partake in the self-assembly of the synthetic cells. To this end, coacervates were centrifugated as previously described, after which a viscous pellet containing the coacervates was obtained.[23,39] After careful removal of the supernatant, the pellet was redispersed in cell culture medium (Figure 5A).

Microscopy revealed that the coacervates retained their spherical morphology, even following this mechanical agitation (Figure 5B). The supernatant seemed to comprise mostly large terpolymer aggregates (Figure 5C). ^{1}H NMR analysis was performed to confirm the composition of supernatant and pellet after the purification step. To this end, coacervates were

https://dx.doi.org/10.1021/acsami.0c19052
ACS Appl. Mater. Interfaces 2021, 13, 7879−7889

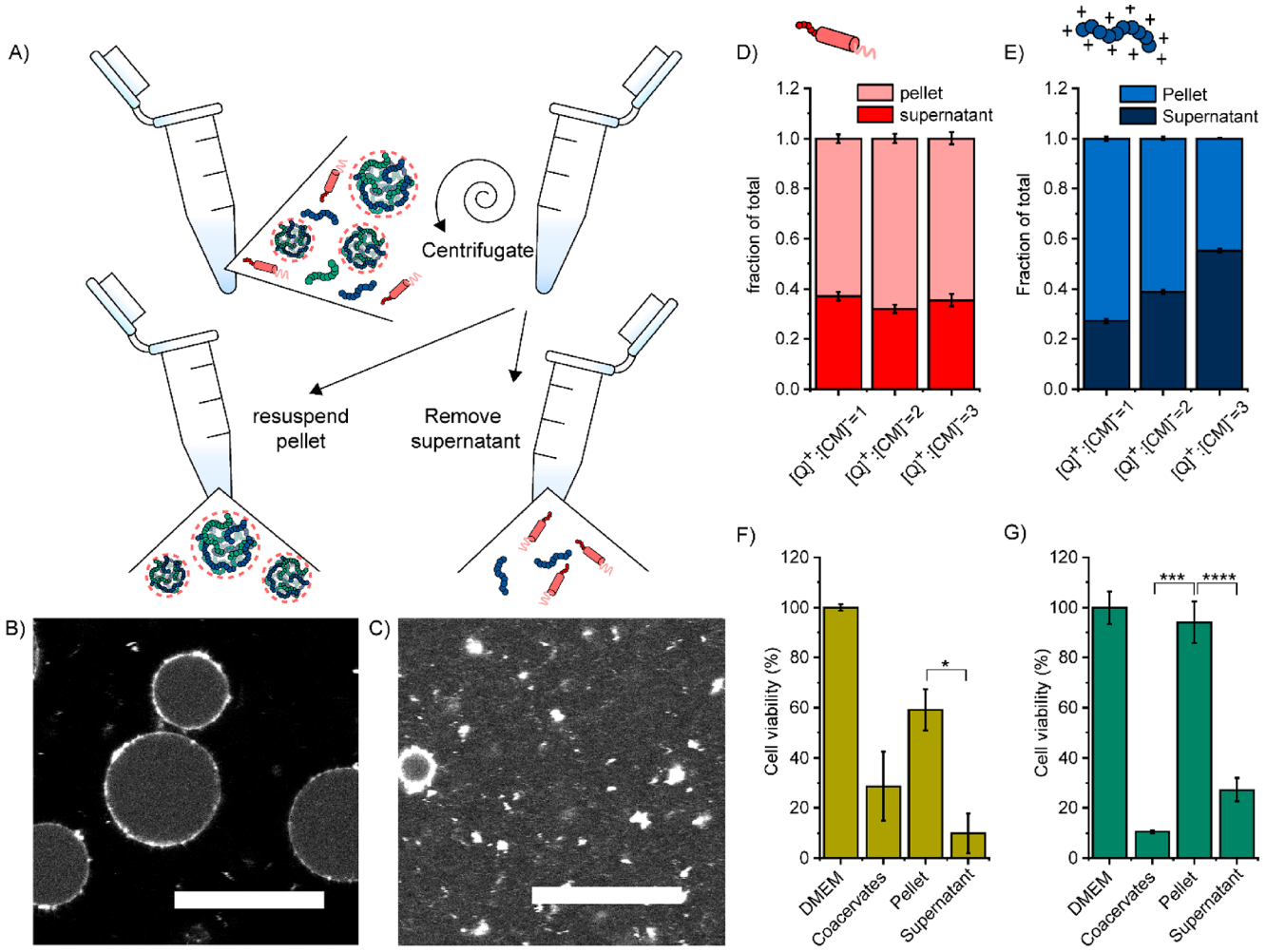

Figure 5. Purification of coacervate-based synthetic cells. (A) Schematic illustrating the purification process of synthetic cells. Coacervates are centrifuged, after which the supernatant is removed, and the purified pellet is redispersed in an equal amount of cell culture medium. (B, C) Confocal microscopy image of purified coacervates prepared using 1.2 mg mL^{-1} terpolymer (final concentration) (B) pellet and (C) supernatant. The terpolymer is visualized with Nile Red. Scale bar represents 25 μm. (D, E) Fraction of compounds present in the pellet and supernatant for (D) terpolymer and (E) Q-amylose. Fractions were calculated from ^{1}H NMR spectra, as the ratio of peak integrals normalized to the control. Error bars represent the standard deviation of 4 different resonances for (D) δ, 2.32−2.22 (t, 2H; CH_2); δ, 2.00−1.85 (m, 2H; CH_2); δ, 1.65−1.45 (m, 4H; CH_2); and δ, 1.35−1.25 (m, 2H; CH_2) (Figure S10A); and 2 different resonances for (E) δ, 4.50−4.35 (m, 1H; CH); and δ, 3.30−3.15 (m, 9H; CH_3) (Figure S10B). (F, G) Cell viability after 24 h of incubation with DMEM, coacervates, purified coacervates, or supernatant for (F) HeLa cells and (G) RAW264.7 cells. $[Q]^+/[CM]^-$ = 3, Q-amylose$_{DS=1.0}$. The Q-amylose and terpolymer concentrations are 0.5 and 1.2 mg mL^{-1}, respectively. Error bars represent the standard deviation of 2 independent experiments. Significance was assessed using the Student's t test. Significance levels are indicated by *p < 0.1, ***p < 0.025, or ****p < 0.01.

prepared as previously described, purified, freeze-dried, and subsequently dissolved in NMR solvent. Integrals of unique compound peaks were used to calculate the ratio of polymer present in the pellet and supernatant, which was normalized to a control (Figure S10 and Tables S1 and S2). Between 35 and 38% of terpolymer was present in the supernatant after purification, regardless of the charge stoichiometry of Q-amylose and CM-amylose (Figure 5D). These data suggest that anchoring of the terpolymer on the coacervate surface is independent of the net charge of the coacervate. This contrasts with the previous hypothesis that a net positive charge is required to attract the negatively charged poly(glutamic acid) block of the terpolymer to the surface of the coacervate. Moreover, between 27 and 55% of Q-amylose was present in the supernatant (Figure 5E). As expected, this fraction increased with increasing charge stoichiometry.

Following this purification step, coacervates and supernatant were added to cells and their toxicity was determined. Interestingly, purification of coacervates restored cell viability to almost 70% for HeLa cells and almost 100% for RAW624.7 cells, indicating a minor role for these particles in toxicity (Figure 5F and G). In contrast, the supernatant with aggregated terpolymer displayed increased toxicity. The increase and decrease of toxicity are independent of charge stoichiometry and DS for HeLa cells (Figure S9A and C) and RAW 264.7 cells (Figure S9B and D). These data indicate that polymer design and coacervate purification using centrifugation are effective methods to improve the biocompatibility of this class of protocells.

CONCLUSIONS

For synthetic cells to be suitable for biological applications, they have to display excellent biocompatibility with living cells.

https://dx.doi.org/10.1021/acsami.0c19052
ACS Appl. Mater. Interfaces 2021, 13, 7879−7889

In this study, the impact of the structure and formulation of our recently developed coacervate-based synthetic cell platform on cell viability was thoroughly examined. Coacervates were initially toxic when prepared using a previously reported formulation. Consequently, the toxicities of Q-amylose, CM-amylose, and terpolymer PEG−PCL-*g*-TMC−PGlu were studied both separately and after self-assembly. CM-amylose displayed no relevant toxicity, while Q-amylose and PEG−PCL-*g*-TMC−PGlu reduced cell viability at concentrations typical for a coacervate-based synthetic cell formulation. In an effort to better understand and improve their biocompatibilities, the coacervate formulation was optimized by varying (i) the charge stoichiometry of Q-amylose and CM-amylose, (ii) the degree of substitution of Q-amylose, and (iii) the concentration of terpolymer. The cell viability could be partially improved by synthesizing a new amylose polymer with a reduced positive charge density. Interestingly, however, not the coacervates but rather the free polymer was primarily responsible for the observed toxicity. The incorporation of a simple purification step to remove free polymers from the coacervate solution proved to be successful in rescuing cell viability.

To address the biomedical challenges of the future, we need to engineer complex and adaptive micrometer-scale particles. While the results described herein are specific to this coacervate-based synthetic cell platform, we illustrate the importance of taking a detailed, component-focused approach toward investigating the viability of complex hierachically assembled systems in close proximity with living cells. Furthermore, these results highlight the exciting potential of this and other modular, engineerable synthetic cell platforms for addressing significant challenges in biomedical engineering, such as tissue culturing and localized release of therapeutics.

■ ASSOCIATED CONTENT

Supporting Information

The Supporting Information is available free of charge at https://pubs.acs.org/doi/10.1021/acsami.0c19052.

NMR characterization of Q-amylose, CM-amylose, and PEG−PCL-*g*-TMC−PGlu, GPC traces of PEG−PCL-*g*-TMC−PGlu, confocal microscopy images of different coacervate-based synthetic cell compositions, and cell viability assays with different compositions of coacervate-based synthetic cells (PDF)

■ AUTHOR INFORMATION

Corresponding Authors

Alexander F. Mason − *Institute for Complex Molecular Systems, Eindhoven University of Technology, 5600MB Eindhoven, The Netherlands;* orcid.org/0000-0002-2847-0253; Email: a.f.mason@tue.nl

Jan C. M. van Hest − *Institute for Complex Molecular Systems, Eindhoven University of Technology, 5600MB Eindhoven, The Netherlands;* orcid.org/0000-0001-7973-2404; Email: j.c.m.v.hest@tue.nl

Authors

Marleen H. M. E. van Stevendaal − *Institute for Complex Molecular Systems, Eindhoven University of Technology, 5600MB Eindhoven, The Netherlands*

Laurynas Vasiukas − *Institute for Complex Molecular Systems, Eindhoven University of Technology, 5600MB Eindhoven, The Netherlands*

N. Amy Yewdall − *Institute for Molecules and Materials, Radboud University, 6525 AJ Nijmegen, The Netherlands*

Complete contact information is available at: https://pubs.acs.org/10.1021/acsami.0c19052

Author Contributions

M.H.M.E.v.S., A.F.M., and J.C.M.v.H. wrote the manuscript. M.H.M.E.v.S., N.A.Y., A.F.M., and J.C.M.v.H. designed the research. M.H.M.E.v.S., L.V., and A.F.M. performed the experiments. All authors reviewed the manuscript.

Funding

This research was funded by the Dutch Ministry of Education, Culture and Science (Gravitation Program 024.001.035) and the ERC Advanced Grant (Artisym 694120).

Notes

The authors declare no competing financial interest.

■ ABBREVIATIONS

DEAE, diethylaminoethyl; PEAD, poly(ethylene argininylaspartate diglyceride); PLL, poly-L-lysine; PEI, poly(ethylene imine); PAH, poly(allyl amine); PDDA, poly(diallyl dimethylammonium); Q, quaternary amine; CM, carboxymethyl; PEG−PCL-*g*-TMC−PGlu, poly(ethylene glycol)−poly((ε-caprolactone)-*gradient*-trimethylene carbonate)−poly(glutamic acid); DS, degree of substitution

■ REFERENCES

(1) Banani, S. F.; Lee, H. O.; Hyman, A. A.; Rosen, M. K. Biomolecular Condensates: Organizers of Cellular Biochemistry. *Nat. Rev. Mol. Cell Biol.* **2017**, *18* (5), 285−298.

(2) Sabari, B. R.; Dall'Agnese, A.; Young, R. A. Biomolecular Condensates in the Nucleus. *Trends Biochem. Sci.* **2020**, *45*, 961−977.

(3) Uversky, V. N. Protein Intrinsic Disorder-Based Liquid-Liquid Phase Transitions in Biological Systems: Complex Coacervates and Membrane-Less Organelles. *Adv. Colloid Interface Sci.* **2017**, *239*, 97−114.

(4) Mason, A. F.; van Hest, J. C. M. Multifaceted Cell Mimicry in Coacervate-Based Synthetic Cells. *Emerg. Top. Life Sci.* **2019**, *3* (5), 567−571.

(5) Yewdall, N. A.; Mason, A. F.; van Hest, J. C. M. The Hallmarks of Living Systems: Towards Creating Artificial Cells. *Interface Focus* **2018**, *8* (5), 20180023.

(6) Wang, L.; Song, S.; van Hest, J.; Abdelmohsen, L. K. E. A.; Huang, X.; Sánchez, S. Biomimicry of Cellular Motility and Communication Based on Synthetic Soft-Architectures. *Small* **2020**, *16* (27), 1907680.

(7) Elani, Y. Interfacing Living and Synthetic Cells as an Emerging Frontier in Synthetic Biology. *Angew. Chem., Int. Ed.* **2020**, DOI: 10.1002/anie.202006941.

(8) Johnson, N. R.; Wang, Y. Coacervate Delivery Systems for Proteins and Small Molecule Drugs. *Expert Opin. Drug Delivery* **2014**, *11* (12), 1829−1832.

(9) Blocher, W. C.; Perry, S. L. Complex Coacervate-Based Materials for Biomedicine. *WIREs Nanomedicine and Nanobiotechnology* **2017**, *9* (4), No. e1442.

(10) Perry, S. L.; Li, Y.; Priftis, D.; Leon, L.; Tirrell, M. The Effect of Salt on the Complex Coacervation of Vinyl Polyelectrolytes. *Polymers* **2014**, *6*, 1756−1772.

(11) Priftis, D.; Laugel, N.; Tirrell, M. Thermodynamic Characterization of Polypeptide Complex Coacervation. *Langmuir* **2012**, *28* (45), 15947−15957.

(12) Oparin, A I. *The Origin of Life*, 2nd ed.; Dover Publications, Inc.: Mineola, NY, 1953.
(13) Deshpande, S.; Brandenburg, F.; Lau, A.; Last, M. G. F.; Spoelstra, W. K.; Reese, L.; Wunnava, S.; Dogterom, M.; Dekker, C. Spatiotemporal Control of Coacervate Formation within Liposomes. *Nat. Commun.* **2019**, *10* (1), 1800.
(14) Deng, N.; Huck, W. T. S. Microfluidic Formation of Monodisperse Coacervate Organelles in Liposomes. *Angew. Chem., Int. Ed.* **2017**, *56* (33), 9736−9740.
(15) Shin, Y.; Brangwynne, C. P. Liquid Phase Condensation in Cell Physiology and Disease. *Science (Washington, DC, U. S.)* **2017**, *357* (6357), eaaf4382.
(16) Buddingh', B. C.; van Hest, J. C. M. Artificial Cells: Synthetic Compartments with Life-like Functionality and Adaptivity. *Acc. Chem. Res.* **2017**, *50* (4), 769−777.
(17) Nakashima, K. K.; Vibhute, M. A.; Spruijt, E. Biomolecular Chemistry in Liquid Phase Separated Compartments. *Frontiers in Molecular Biosciences.* **2019**, *6*, 21.
(18) Altenburg, W. J.; Yewdall, N. A.; Vervoort, D. F. M.; van Stevendaal, M. H. M.; Mason, A. F.; van Hest, J. C. M. Programmed Spatial Organization of Biomacromolecules into Discrete, Coacervate-Based Protocells. *Nat. Commun.* **2020**, *11*, 11.
(19) Williams, D. S.; Koga, S.; Hak, C. R. C.; Majrekar, A.; Patil, A. J.; Perriman, A. W.; Mann, S. Polymer/Nucleotide Droplets as Bio-Inspired Functional Micro-Compartments. *Soft Matter* **2012**, *8* (22), 6004−6014.
(20) Tang, T.-Y. D.; Antognozzi, M.; Vicary, J. A.; Perriman, A. W.; Mann, S. Small-Molecule Uptake in Membrane-Free Peptide/Nucleotide Protocells. *Soft Matter* **2013**, *9* (31), 7647−7656.
(21) Drobot, B.; Iglesias-Artola, J. M.; Le Vay, K.; Mayr, V.; Kar, M.; Kreysing, M.; Mutschler, H.; Tang, T.-Y. D. Compartmentalised RNA Catalysis in Membrane-Free Coacervate Protocells. *Nat. Commun.* **2018**, *9* (1), 3643.
(22) Pippa, N.; Karayianni, M.; Pispas, S.; Demetzos, C. Complexation of Cationic-Neutral Block Polyelectrolyte with Insulin and in Vitro Release Studies. *Int. J. Pharm.* **2015**, *491* (1), 136−143.
(23) Yewdall, N. A.; Buddingh, B. C.; Altenburg, W. J.; Timmermans, S. B. P. E.; Vervoort, D. F. M.; Abdelmohsen, L. K. E. A.; Mason, A. F.; van Hest, J. C. M. Physicochemical Characterization of Polymer-Stabilized Coacervate Protocells. *ChemBioChem* **2019**, *20* (20), 2643−2652.
(24) Schuster, B. S.; Reed, E. H.; Parthasarathy, R.; Jahnke, C. N.; Caldwell, R. M.; Bermudez, J. G.; Ramage, H.; Good, M. C.; Hammer, D. A. Controllable Protein Phase Separation and Modular Recruitment to Form Responsive Membraneless Organelles. *Nat. Commun.* **2018**, *9* (1), 2985.
(25) Faltova, L.; Küffner, A. M.; Hondele, M.; Weis, K.; Arosio, P. Multifunctional Protein Materials and Microreactors Using Low Complexity Domains as Molecular Adhesives. *ACS Nano* **2018**, *12* (10), 9991−9999.
(26) Awada, H. K.; Long, D. W.; Wang, Z.; Hwang, M. P.; Kim, K.; Wang, Y. A Single Injection of Protein-Loaded Coacervate-Gel Significantly Improves Cardiac Function Post Infarction. *Biomaterials* **2017**, *125*, 65−80.
(27) Lim, Z. W.; Ping, Y.; Miserez, A. Glucose-Responsive Peptide Coacervates with High Encapsulation Efficiency for Controlled Release of Insulin. *Bioconjugate Chem.* **2018**, *29* (7), 2176−2180.
(28) Aumiller, W. M.; Pir Cakmak, F.; Davis, B. W.; Keating, C. D. RNA-Based Coacervates as a Model for Membraneless Organelles: Formation, Properties, and Interfacial Liposome Assembly. *Langmuir* **2016**, *32* (39), 10042−10053.
(29) Kayitmazer, A. B.; Koksal, A. F.; Kilic Iyilik, E. Complex Coacervation of Hyaluronic Acid and Chitosan: Effects of PH, Ionic Strength, Charge Density, Chain Length and the Charge Ratio. *Soft Matter* **2015**, *11* (44), 8605−8612.
(30) Zhang, Y.; Liu, S.; Yao, Y.; Chen, Y.; Zhou, S.; Yang, X.; Wang, K.; Liu, J. Invasion and Defense Interactions between Enzyme-Active Liquid Coacervate Protocells and Living Cells. *Small* **2020**, *16* (29), 2002073.
(31) Black, K. A.; Priftis, D.; Perry, S. L.; Yip, J.; Byun, W. Y.; Tirrell, M. Protein Encapsulation via Polypeptide Complex Coacervation. *ACS Macro Lett.* **2014**, *3* (10), 1088−1091.
(32) Fischer, D.; Li, Y.; Ahlemeyer, B.; Krieglstein, J.; Kissel, T. In Vitro Cytotoxicity Testing of Polycations: Influence of Polymer Structure on Cell Viability and Hemolysis. *Biomaterials* **2003**, *24* (7), 1121−1131.
(33) Winslow, B. D.; Shao, H.; Stewart, R. J.; Tresco, P. A. Biocompatibility of Adhesive Complex Coacervates Modeled after the Sandcastle Glue of Phragmatopoma Californica for Craniofacial Reconstruction. *Biomaterials* **2010**, *31* (36), 9373−9381.
(34) Karabiyik Acar, O.; Kayitmazer, A. B.; Torun Kose, G. Hyaluronic Acid/Chitosan Coacervate-Based Scaffolds. *Biomacromolecules* **2018**, *19* (4), 1198−1211.
(35) Hwang, M. P.; Ding, X.; Gao, J.; Acharya, A. P.; Little, S. R.; Wang, Y. A Biocompatible Betaine-Functionalized Polycation for Coacervation. *Soft Matter* **2018**, *14* (3), 387−395.
(36) Chu, H.; Gao, J.; Wang, Y. Design, Synthesis, and Biocompatibility of an Arginine-Based Polyester. *Biotechnol. Prog.* **2012**, *28* (1), 257−264.
(37) Mason, A. F.; Buddingh', B. C.; Williams, D. S.; van Hest, J. C. M. Hierarchical Self-Assembly of a Copolymer-Stabilized Coacervate Protocell. *J. Am. Chem. Soc.* **2017**, *139* (48), 17309−17312.
(38) Tanaka, T.; Nagai, H.; Noguchi, M.; Kobayashi, A.; Shoda, S. One-Step Conversion of Unprotected Sugars to β-Glycosyl Azides Using 2-Chloroimidazolinium Salt in Aqueous Solution. *Chem. Commun.* **2009**, No. 23, 3378.
(39) Mason, A. F.; Altenburg, W. J.; Song, S.; van Stevendaal, M.; van Hest, J. C. M. Terpolymer-Stabilized Complex Coacervates: A Robust and Versatile Synthetic Cell Platform. *Methods Enzymol.* **2021**, *646*, 51−82.
(40) Steensma, D. P.; Timm, M.; Witzig, T. E. *Flow Cytometric Methods for Detection and Quantification of Apoptosis BT - Novel Anticancer Drug Protocols*; Buolamwini, J. K., Adjei, A. A., Eds.; Humana Press: Totowa, NJ, 2003; pp 323−332; DOI: 10.1385/1-59259-380-1:323.
(41) Liu, G.; Li, Y.; Yang, L.; Wei, Y.; Wang, X.; Wang, Z.; Tao, L. Cytotoxicity Study of Polyethylene Glycol Derivatives. *RSC Adv.* **2017**, *7* (30), 18252−18259.
(42) Verheijen, M.; Lienhard, M.; Schrooders, Y.; Clayton, O.; Nudischer, R.; Boerno, S.; Timmermann, B.; Selevsek, N.; Schlapbach, R.; Gmuender, H.; Gotta, S.; Geraedts, J.; Herwig, R.; Kleinjans, J.; Caiment, F. DMSO Induces Drastic Changes in Human Cellular Processes and Epigenetic Landscape in Vitro. *Sci. Rep.* **2019**, *9* (1), 4641.
(43) Stern, S. T.; Adiseshaiah, P. P.; Crist, R. M. Autophagy and Lysosomal Dysfunction as Emerging Mechanisms of Nanomaterial Toxicity. *Part. Fibre Toxicol.* **2012**, *9*, 20.
(44) van Oppen, L. M. P. E.; Abdelmohsen, L. K. E. A.; van Emst-de Vries, S. E.; Welzen, P. L. W.; Wilson, D. A.; Smeitink, J. A. M.; Koopman, W. J. H.; Brock, R.; Willems, P. H. G. M.; Williams, D. S.; van Hest, J. C. M. Biodegradable Synthetic Organelles Demonstrate ROS Shielding in Human-Complex-I-Deficient Fibroblasts. *ACS Cent. Sci.* **2018**, *4* (7), 917−928.
(45) Cao, S.; Shao, J.; Xia, Y.; Che, H.; Zhong, Z.; Meng, F.; van Hest, J. C. M.; Abdelmohsen, L. K. E. A.; Williams, D. S. Molecular Programming of Biodegradable Nanoworms via Ionically Induced Morphology Switch toward Asymmetric Therapeutic Carriers. *Small* **2019**, *15* (38), 1901849.
(46) Fröhlich, E. The Role of Surface Charge in Cellular Uptake and Cytotoxicity of Medical Nanoparticles. *Int. J. Nanomed.* **2012**, *7*, 5577−5591.
(47) Kamiński, K.; Kałaska, B.; Koczurkiewicz, P.; Michalik, M.; Szczubiałka, K.; Mogielnicki, A.; Buczko, W.; Nowakowska, M. New Arginine Substituted Derivative of Poly(Allylamine Hydrochloride) for Heparin Reversal. *MedChemComm* **2014**, *5* (4), 489−495.
(48) Inácio, Â. S.; Costa, G. N.; Domingues, N. S.; Santos, M. S.; Moreno, A. J. M.; Vaz, W. L. C.; Vieira, O. V. Mitochondrial Dysfunction Is the Focus of Quaternary Ammonium Surfactant

https://dx.doi.org/10.1021/acsami.0c19052
ACS Appl. Mater. Interfaces 2021, 13, 7879−7889

Toxicity to Mammalian Epithelial Cells. *Antimicrob. Agents Chemother.* **2013**, *57* (6), 2631−2639.
(49) Monnery, B. D.; Wright, M.; Cavill, R.; Hoogenboom, R.; Shaunak, S.; Steinke, J. H. G.; Thanou, M. Cytotoxicity of Polycations: Relationship of Molecular Weight and the Hydrolytic Theory of the Mechanism of Toxicity. *Int. J. Pharm.* **2017**, *521* (1), 249−258.
(50) Chen, B.; Le, W.; Wang, Y.; Li, Z.; Wang, D.; Ren, L.; Lin, L.; Cui, S.; Hu, J. J.; Hu, Y.; Yang, P.; Ewing, R. C.; Shi, D.; Cui, Z. Targeting Negative Surface Charges of Cancer Cells by Multifunctional Nanoprobes. *Theranostics* **2016**, *6* (11), 1887−1898.
(51) dos Santos, T.; Varela, J.; Lynch, I.; Salvati, A.; Dawson, K. A. Quantitative Assessment of the Comparative Nanoparticle-Uptake Efficiency of a Range of Cell Lines. *Small* **2011**, *7* (23), 3341−3349.

https://dx.doi.org/10.1021/acsami.0c19052
ACS Appl. Mater. Interfaces 2021, 13, 7879−7889